Spin transport in graphene - hexagonal boron nitride van der Waals heterostructures

Gurram, Mallikarjuna

Chapter 2

Concepts of spintronics

Abstract

This chapter introduces the concepts required to understand the electrical spin injection, transport, and detection in nonmagnetic materials. First, a brief introduction is given to the basic properties of ferromagnetic and non-magnetic materials that are necessary to understand the physics of electrical spin transport. This is followed by introducing the two channel model of spin injection across a ferromagnet/nonmagnet interface followed by derivation of an expression for the spin injection polarization. Thereafter a general solution to the one dimensional Bloch diffusion equation is given using which the expressions for spin valve and Hanle spin precession signals in the four-terminal nonlocal and two-terminal geometries are given. A brief account on the various definitions of spin polarizations used in literature is also given for a clear understanding. In the end, different kinds of spin relaxation mechanisms are discussed.

2.1 Elementary concepts of spin transport

In standard spin transport formalism, one makes an assumption that up-spin and down-spin electrons diffuse independently with a weak scattering interactions between both types of spins. The transport of two spin types can be treated separately [1] with different diffusion constants $D_{\uparrow(\downarrow)}$, conductivities $\sigma_{\uparrow(\downarrow)}$, and density of states (DoS) $g_{\uparrow(\downarrow)}$. For a conductor having an electrical current flow due to an electrostatic potential, one can define the following characteristics:

1. **Chemical potential:** Spin accumulation or spin chemical potential ($\mu_{\rm s}$) is the difference between the chemical potentials of the up-spin ($\mu_\uparrow$) and the down-spin ($\mu_\downarrow$), and the net charge chemical potential (μ) is the average of spin dependent electrochemical potentials. All these quantities are related as,

$$\begin{aligned} \mu &= (\mu_\uparrow + \mu_\downarrow)/2, \\ \mu_{\rm s} &= (\mu_\uparrow - \mu_\downarrow)/2, \\ \mu_{\uparrow(\downarrow)} &= \mu + (-)\mu_{\rm s}. \end{aligned} \tag{2.1}$$

2. **Magnetization:** Magnetization (M) is defined by the difference between the

number of up-spin ($n_\uparrow$) and down-spin ($n_\downarrow$) electrons, given by

$$M = \mu_B(n_\uparrow - n_\downarrow), \tag{2.2}$$

assuming each electron has a magnetic moment of one Bohr magneton, μ_B.

3. **Conductivity:** The conductivity of each spin channel, $\sigma_{\uparrow(\downarrow)}$, is related to the density of states $g_{\uparrow(\downarrow)}$ at the Fermi energy E_f, $g_{\uparrow(\downarrow)}(E_\mathrm{f})$, and the diffusion coefficient $D_{\uparrow(\downarrow)}$ via the Einstein relation,

$$\sigma_{\uparrow(\downarrow)} = g_{\uparrow(\downarrow)}(E_\mathrm{f})e^2 D_{\uparrow(\downarrow)} \tag{2.3}$$

The diffusivity of each spin channel, $D_{\uparrow(\downarrow)}$, is related to the spin dependent Fermi velocity $v_{F\uparrow(\downarrow)}$ and the mean free path length $l_{mfp\uparrow(\downarrow)}$, given by $D_{\uparrow(\downarrow)} = (v_{F\uparrow(\downarrow)} l_{mfp\uparrow(\downarrow)})/3$ where the dimensionality of a three dimensional system is given by the factor $1/3$.

4. **Current:** The electrical current for two spins $j_{\uparrow(\downarrow)}$ is driven by the gradient of the electric potential ∇V and the gradient of the carrier density $\nabla \delta n_{\uparrow(\downarrow)}$,

$$j_{\uparrow(\downarrow)} = -\sigma_{\uparrow(\downarrow)} \nabla V + eD_{\uparrow(\downarrow)} \nabla \delta n_{\uparrow(\downarrow)} \tag{2.4}$$

with a deviation in the carrier density from equilibrium $\delta n_{\uparrow(\downarrow)} = g_{\uparrow(\downarrow)} \delta\mu$, where $\delta\mu$ is a shift in the chemical potential of charge carriers from its equilibrium value.

From the above equations, the individual spin current densities can be obtained as

$$j_{\uparrow(\downarrow)} = \frac{\sigma_{\uparrow(\downarrow)}}{e} \nabla \mu_{\uparrow(\downarrow)} \tag{2.5}$$

where $\mu_{\uparrow(\downarrow)} = \delta\mu - eV$ is the electrochemical potential of the up-spin, $\uparrow$(down-spin, $\downarrow$) subbands.

According to Ohm's law, a charge current flow is driven by an electric field, E and is given by $j = \sigma E = -\sigma \nabla V$.

5. **Polarization:** A charge current density (j) can be written as a sum of up-spin current density ($j_\uparrow$) and down-spin current density ($j_\downarrow$), the spin current density (j_s), and the current spin polarization P_j are defined as:

$$P_j = \frac{j_\mathrm{s}}{j} = \frac{j_\uparrow - j_\downarrow}{j_\uparrow + j_\downarrow} = \frac{\sigma_\mathrm{s} \nabla\mu + \sigma \nabla \mu_\mathrm{s}}{\sigma \nabla\mu + \sigma_\mathrm{s} \nabla \mu_\mathrm{s}} \tag{2.6}$$

where the charge conductance σ, spin conductance σ_s, and the conductance spin polarization P_σ are given by,

$$P_\sigma = \frac{\sigma_\mathrm{s}}{\sigma} = \frac{\sigma_\uparrow - \sigma_\downarrow}{\sigma_\uparrow + \sigma_\downarrow} \tag{2.7}$$

For different DoS at the Fermi level, one can define the total charge DoS (g), spin DoS (g_s), and the density-of-states spin polarization (P_g) as,

$$P_g = \frac{g_s}{g} = \frac{g_\uparrow - g_\downarrow}{g_\uparrow + g_\downarrow} \tag{2.8}$$

Spin transport is characterized by the spin currents due to up-spin ($j_\uparrow$) and down-spin ($j_\downarrow$), and its spin polarization is commonly expressed in terms of current spin polarization P_j, and conductivity spin polarization P_σ. Therefore, the charge and spin current densities (Eq. 2.6) can be written in terms of spin polarizations as,

$$\begin{aligned} j &= P_\sigma j_s + \sigma(1 - P_\sigma^2)\nabla\mu, \\ j_s &= P_\sigma j + \sigma(1 - P_\sigma^2)\nabla\mu_s, \\ P_j &= P_\sigma + \frac{\sigma(1 - P_\sigma^2)}{j}\nabla\mu_s \end{aligned} \tag{2.9}$$

6. **Drift-Diffusion equation:** The transport of spins is described by the spin drift-diffusion equation [2],

$$D_s \bigtriangledown^2 \mu_s - \frac{\mu_s}{\tau} + \omega_L \times \mu_s = \frac{d\mu_s}{dt} = 0 \tag{2.10}$$

where $\mu_s = \mu_{sx}\hat{x} + \mu_{sy}\hat{y} + \mu_{sz}\hat{z}$ represents the spin accumulation in three dimensions, D_s is the spin diffusion constant, τ_s is the spin relaxation time, and $\omega_L = \frac{g\mu_B B}{\hbar}$ is the Larmor spin precession frequency caused by the magnetic field B with, Bohr magneton μ_B, and the gyromagnetic factor g(=2 for electrons). In the steady state ($\frac{d\mu_s}{dt} = 0$) under no external influence on spins, the solution to the above equation for one-dimensional spin transport, say along the x-direction, is given by,

$$\begin{aligned} \bigtriangledown^2\mu_s &= \frac{\mu_s}{\lambda_s^2} \\ \mu_{sx}(x) &= Ae^{-\frac{x}{\lambda_s}} + Be^{+\frac{x}{\lambda_s}} \end{aligned} \tag{2.11}$$

where, $\lambda_s = \sqrt{D_s\tau_s}$ is the spin relaxation length. For a given set of boundary conditions, the values of A and B can be evaluated. See Appendix A for special case of a nonlocal spin transport geometry.

2.2 Standard model of spin injection: a F/N contact

2.2.1 Ferromagnetic materials

Ferromagnetism is a result of collective ordering of electron spins in a material. Depending on the material, this phenomenon persists below a certain temperature,

called Curie temperature. The specific ordering of different electrons' magnetic moments in a Ferromagnet (F) is regarded as a purely quantum mechanical effect caused by an exchange interaction between the magnetic moments. An exchange interaction arises due to Pauli exclusion principle and Coulomb interaction between electrons.

According to the Stoner model, a combination of a strong Coulomb exchange interaction and a large DoS at the Fermi level leads to a spontaneous ferromagnetism. This criterion is met for the 3d transition metal ferromagnets, Fe, Ni, and Co. In these ferromagnets, the strong exchange interaction leads to different DoS for electrons with up-spin(↑) and down-spin(↓). As a result, up-spin and down-spin bands are split spontaneously without needing any external magnetic field, creating a equilibrium distribution of spins, which is commonly referred to as spin imbalance or spin splitting of the DoS.

Electrical transport in a ferromagnetic metal is characterized by the conduction electrons at the Fermi-level (E_{f}). Since the electrons with up-spin and down-spin have different DoS at E_{f}, they both have different conductivities (Eq. 2.3). In the diffusive regime, conductivities of two spin types in a ferromagnet $\sigma^{\mathrm{F}}_{\uparrow(\downarrow)}$ can be evaluated using the Einstein relation (Eq. 2.3).

Another property of the ferromagnet pertaining to the unequal density of each spin type conduction electrons at the Fermi level is the degree of spin polarization (P). It is usually given by the difference between the DoS of the majority spin and the minority spin at the Fermi level, where the majority and minority refers to the spin of the larger and smaller total electron density. For simplicity, the convention followed here is: the up-spin is referred to the majority spin which determines the magnetization and the down-spin is referred to the minority spin. The DoS polarization of a ferromagnet P^{F}_{g} can be written by Eq. 2.8.

Let us consider a ferromagnet in contact with a non-magnet (N) where an electric current is driven from F to N [Fig. 2.1]. The transport of non-equilibrium spins in F can be described by the diffusion equation 2.11 whose solution is given by: $\mu^{\mathrm{F}}_{\mathrm{s}}(z) = \mu^{\mathrm{F}}_{\mathrm{s}}(0)e^{-\frac{z}{\lambda^{\mathrm{F}}_{\mathrm{S}}}}$, as $\mu^{\mathrm{F}}_{\mathrm{s}}(z \to \infty) \to 0$. Therefore, the current spin polarization of F, P^{F}_{j}, can be written as (using Eq.2.9),

$$P^{\mathrm{F}}_{j} = P^{\mathrm{F}}_{\sigma} - \frac{1}{j^{\mathrm{F}}}\frac{\mu^{\mathrm{F}}_{\mathrm{s}}(z)}{R^{\mathrm{F}}} \tag{2.12}$$

where R^{F} is the effective resistance of F.

Note that the individual values of P^{F}_{j} and P^{F}_{σ} of a ferromagnet cannot be measured directly. One need to calculate or estimate them from an indirect measurement, for example, via tunneling conductance measurements for superconductor(SuC)/Insulator(I)/F vetical tunneling junctions [3].

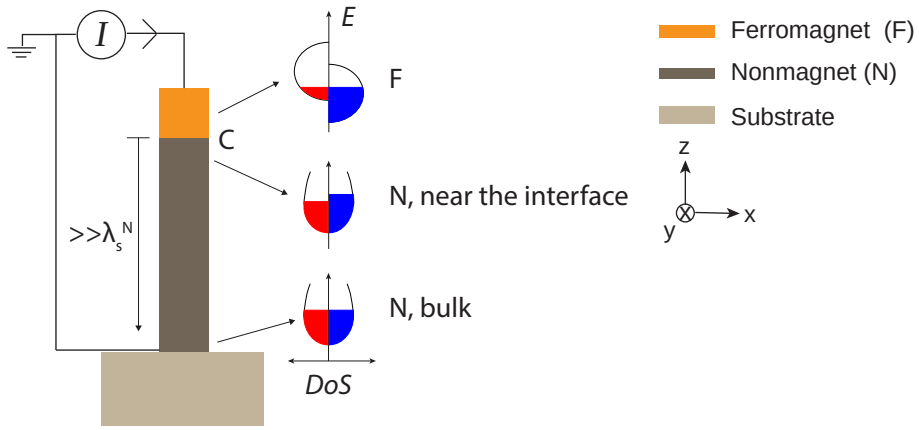

Figure 2.1: Electrical spin injection from a ferromagnet (F) into a nonmagnet (N) across an isolated F/N junction using a current source I. The contact region of the F/N junction denoted by 'C'. Band diagrams represents the density of states (DoS) of F and N. Due to unequal DoS in F, a non-equilibrium spin accumulation is injected into N near the F/N interface which will decay into the bulk of N where the equilibrium spin accumulation is zero.

2.2.2 Nonmagnetic materials

In equilibrium, nonmagnetic materials (N) have an equal number of up-spin and down-spin electrons, i.e., $P_g = 0$, $P_\sigma = 0$, and $\mu_s = 0$.

However, it is possible to create a non-equilibrium spin accumulation in N by injecting an already spin polarized current. This can be achieved by passing an electrical current through F into N (Fig. 2.1). As a result a non-equilibrium spin accumulation μ_s^N will be created at the F/N interface (C). The region of N far from the interface is at equilibrium with $\mu_s^N = 0$. This difference in spin chemical potential in N, between the regions close to and far from the F/N contact, drives the spin current in N.

The transport of non-equilibrium spins in N can be described by the diffusion equation 2.11 whose solution is given by: $\mu_s^N(z) = \mu_s^N(0)e^{\frac{z}{\lambda_s^N}}$, as $\mu_s^N(z \to -\infty) \to 0$. Therefore, the current spin polarization of N can be written as (using Eq. 2.9),

$$P_j^N = \frac{1}{j^N}\frac{\mu_s^N(z)}{R^N} \tag{2.13}$$

where R^N is the effective resistance of N.

2.2.3 Spin current across an F/N interface

Charge and spin transport across an interface (C) between two dissimilar materials can be described by considering a difference in the chemical potentials across interface. The conductivity spin polarization P_σ^{C} and the current spin polarization P_j^{C} of a F/N contact are related by,

$$P_j^{\mathrm{C}} = P_\sigma^{\mathrm{C}} + \frac{1}{j^{\mathrm{C}}} \frac{[\mu_{\mathrm{s}}^{\mathrm{F}}(0) - \mu_{\mathrm{s}}^{\mathrm{N}}(0)]}{R^{\mathrm{C}}} \tag{2.14}$$

where R^{C} is the effective resistance of the F/N contact

2.2.4 Spin injection polarization: a F/N contact

Assuming the spin current and charge current conservation across the F/N contact, i.e., the continuity of the charge current j and the spin current j_{s}, we can find the current spin injection polarization $P_{\mathrm{in}}^{\mathrm{C}}$ of the F/N contact, defined as $P_j^{\mathrm{C}} = P_{\mathrm{in}}^{\mathrm{C}} = \frac{j_{\mathrm{s}}}{j}$, (using Eqs. 2.12, 2.13, and 2.14),

$$P_j^{\mathrm{C}} = P_{\mathrm{in}}^{\mathrm{C}} = \frac{P_\sigma^{\mathrm{F}} R^{\mathrm{F}} + P_\sigma^{\mathrm{C}} R^{\mathrm{C}}}{R^{\mathrm{F}} + R^{\mathrm{C}} + R^{\mathrm{N}}} \tag{2.15}$$

This is an important factor for characterizing the spin injection efficiency of a contact. More about this parameter will be discussed in the following section 2.5.

When the direction of the current is reversed (Fig. 2.1), the spins will flow from N to F across the F/N contact. Now, the figure of merit for the efficiency of the spin flow across the F/N junction is called spin extraction. For an isolated vertical F/N contact, as shown in Fig. 2.1, spin injection and spin extraction processes are equivalent.

2.3 Spin transport in a nonmagnetic channel

Nonmagnetic diffusion channel: The transport of spins in N can be described by considering two spin current channels for up-spin and down-spin [1], using the spin drift-diffusion equation 2.10. Let us consider a nonlocal lateral spin valve geometry as shown in Fig. 2.2 where a current I is injected into the nonmagnet N via ferromagnet at x=0. This geometry consists of three building blocks, namely, ferromanget (F), nonmagnetic channel (N), and F/N interface contacts (C). F1(F2) and C1(C2) denote the ferromagnet and the F/N contact, respectively, at x=0(x=L). A charge current I^{N} in N flows left (along -$\hat{x}$) to the injection point, say at x=0, while the injected spin current $I_{\mathrm{s}}^{\mathrm{N}}$ flows in both directions (along -$\hat{x}$ and +$\hat{x}$) along the length of N. A voltage V_{nl} is measured between the contact at x=L and the reference contact situated far and the corresponding nonlocal resistance is $R_{\mathrm{nl}} = \frac{V_{\mathrm{nl}}}{I}$.

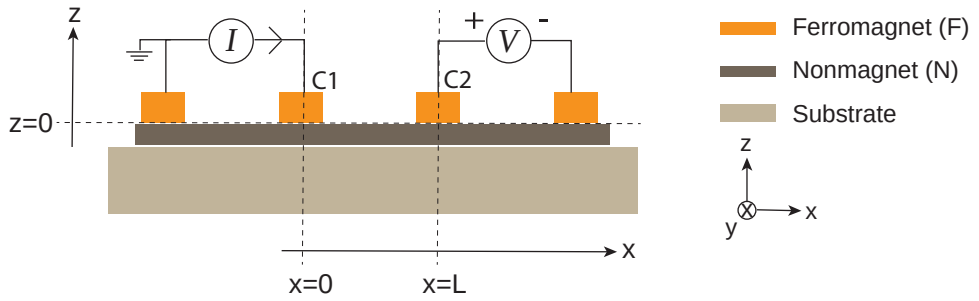

Figure 2.2: Four-terminal non-local spin transport measurement geometry. A current I is driven across two injector contacts and the non-local voltage V is measured across two detector contacts. Inner-injector F/N contact at x=0 is denoted by 'C1' and the inner-detector F/N contact at x=L by 'C2'.

The nonlocal detection voltage $V_{\rm nl}$ depends on the spin accumulation in N at x=L, $\mu_{\rm s}^{\rm N}(x=L)$ that is being diffused from its injection point at x=0 (see Appendix A for the derivation),

$$V_{\rm nl} = -\frac{P_\sigma^{\rm F2} R^{\rm F2} + P_\sigma^{\rm C2} R^{\rm C2}}{R^{\rm F2} + R^{\rm C2}} \mu_{\rm s}^{\rm N}(x=L), \tag{2.16}$$

To obtain $\mu_{\rm s}^{\rm N}(x=L)$ in Eq. 2.16, consider a general case where the spins also precess in the presence of an external magnetic field applied normal to device plane, i.e, **B** = $B_z\hat{z}$. Transport of spin accumulation in N satisfies the steady-state Bloch diffusion equation Eq. 2.10, which describes the diffusion of spin accumulation $\mu_{\rm s}^{\rm N} = \mu_{\rm sx}^{\rm N}\hat{x} + \mu_{\rm sy}^{\rm N}\hat{y} + \mu_{\rm sz}^{\rm N}\hat{z}$ in three-dimensions (3D). However, in the case of an atomically thin N materials like graphene, spin diffusion in the direction normal to the surface can be ignored, limiting the diffusion to 2D. Moreover, the spin injection is assumed to be uniform across the F/N interface, reducing the description of the spin diffusion further to 1D.

Consider the 1D spin diffusion in N, say, along x-direction. We can solve the diffusion equation Eq. 2.10 for the steady state ($\frac{d\mu_{\rm s}^{\rm N}}{dt}$=0) under the boundary conditions $\mu_{sx,sy,sz}^{\rm N}(x \longrightarrow \pm\infty) \longrightarrow 0$, resulting in (see Appendix A for detailed derivation),

$$R_{\rm nl} = \pm\frac{1}{2} P_{\rm in}^{\rm C1} P_{\rm d}^{\rm C2} R^{\rm N} \Re\left\{ \lambda^{\rm N} k_2 \frac{4e^{-k_2 L}}{(1+2r_1k_2)(1+2r_2k_2) - e^{-2k_2 L}} \right\} \left[\frac{R_1 R_2}{R^{\rm N2}}\right], \tag{2.17}$$

Here, $\Re$ denotes the real part, $P_{\rm in}^{\rm C1}$ is the current spin injection polarization, $P_{\rm d}^{\rm C2}$ is the spin detection polarization, $k_2 = \frac{1}{\lambda^{\rm N}}\frac{1}{1+j\omega\tau}$, the r_i and R_i parameters with i=1 for contact at x=0 and i=2 for contact at x=L are given by $r_i = W^{\rm N}\sigma^{\rm N}(R^{\rm Fi} + R^{\rm Ci})$, and $R_i = R^{\rm Fi} + R^{\rm Ci} + R^{\rm N}$ where $R^{\rm F}$, $R^{\rm C}$, and $R^{\rm N}$ represent the effective resistances of F, C, and N, respectively The signs $\pm$ indicate the relative magnetization orientation of the

electrodes, '+' for parallel(P, ↑↑) and '−' for anti-parallel(AP, ↑↓). The magnitude of spin signal is given by $\triangle R_{\rm s} = |\frac{R_{\rm nl}^{\uparrow\uparrow} - R_{\rm nl}^{\uparrow\downarrow}}{2}|$.

The expressions for $P_{\rm in}^{\rm C1}$ [Eq. A.1] and $P_{\rm d}^{\rm C2}$ [Eq. A.14] are given by,

$$\begin{aligned} P_{\rm in}^{\rm C1} &= \frac{I_{\rm s}^{\rm N}}{I} = \frac{P_\sigma^{\rm F1} R^{\rm F1} + P_\sigma^{\rm C1} R^{\rm C1}}{R^{\rm F1} + R^{\rm C1} + R^{\rm N}}, \\ P_{\rm d}^{\rm C2} &= \frac{V}{\mu_{\rm s}^{\rm N}(x=L)} = \frac{P_\sigma^{\rm F2} R^{\rm F2} + P_\sigma^{\rm C2} R^{\rm C2}}{R^{\rm F2} + R^{\rm C2}} \equiv P_{\rm in}^{\rm C2} \frac{R^{\rm F2} + R^{\rm C2} + R^{\rm N}}{R^{\rm F2} + R^{\rm C2}}, \end{aligned} \tag{2.18}$$

2

2.3.1 Four-terminal nonlocal Hanle measurements

Hanle measurements are analyzed for determining the accurate spin transport parameters of transport channel N. For the Hanle measurements, a magnetic field B_z is applied perpendicular to the injected spin direction as a result of which spins precess while travelling through N channel. For tunnel contacts, $R^{\rm C} \gg (R^{\rm F}, R^{\rm N})$. This gives $r \sim W^{\rm N}\sigma^{\rm N}R^{\rm C} \equiv \frac{R^{\rm C}}{R^{\rm N}}\lambda^{\rm N}$, $P_{\rm in}^{\rm C1}P_{\rm d}^{\rm C2} \sim P_\sigma^{\rm C1}P_\sigma^{\rm C2}$ (Eq. 2.18), and the nonlocal resistance (Eq. 2.17) can be written as,

$$R_{\rm nl}(B) = \pm\frac{1}{2} P_{\rm in}^{\rm C1} P_{\rm d}^{\rm C2} R^{\rm N} \Re\left\{ \frac{e^{-\frac{L}{\lambda^{\rm N}}\sqrt{1+i\omega\tau}}}{\sqrt{1+i\omega\tau}} \right\} \tag{2.19}$$

which has the same form as found by Johnson and Silsbee(Eq. (B20), Ref. [4]). Sosenko *et al*. [5] have also derived the same expression and concluded that fitting the Hanle measurement data with the above equation was found to give results equivalent to fitting with the Greeen's function solution [6] of the diffusion equation 2.10 over time:

$$R_{\rm nl}(B) = \pm H_0 \int_0^\infty \frac{e^{-\frac{t}{\tau}}}{\sqrt{4\pi D t}} e^{-\frac{L^2}{4Dt}} cos(\omega t) dt \tag{2.20}$$

An explicit integral of Eq. 2.20 using $Mathematica^{TM}$ program yields the same analytical expression [7] as Eq. 2.19 with $H_0 = P_{\rm in}^{\rm C1}P_{\rm d}^{\rm C2}R^{\rm N}\frac{D}{\lambda^{\rm N}}$.

2.3.2 Four-terminal nonlocal spin valve measurements

For a nonlocal spin valve measurement, B_z=0 ⇒ ω=0. Then $k_2 = \frac{1}{\lambda^{\rm N}}$. The measured spin valve non-local resistance (Eq. 2.17) can be written as,

$$R_{\rm nl} = \pm\frac{1}{2} P_{\rm in}^{\rm C1} P_{\rm d}^{\rm C2} R^{\rm N} \left\{ \frac{\frac{2r_1}{\lambda^{\rm N}}\frac{2r_2}{\lambda^{\rm N}} e^{-\frac{L}{\lambda^{\rm N}}}}{(1+\frac{2r_1}{\lambda^{\rm N}})(1+\frac{2r_2}{\lambda^{\rm N}}) - e^{-2\frac{L}{\lambda^{\rm N}}}} \right\} \left[\frac{R_1}{R^{\rm F1}+R^{\rm C1}} \frac{R_2}{R^{\rm F2}+R^{\rm C2}} \right] \tag{2.21}$$

which has a similar form as of Eq. (3) in Takahashi *et al*. [8] and Eq. (3) in Popinciuc *et al*. [9].

For tunnel contacts, the above equation can be further simplified into,

$$R_{\rm nl} = \pm\frac{1}{2}P_{\rm in}^{\rm C1}P_{\rm d}^{\rm C2}R^{\rm N}e^{-\frac{L}{\lambda^{\rm N}}} \tag{2.22}$$

which agrees with Eq. 6 in Takahashi *et al*. [8].

The four-terminal nonlocal geometry can be used for all-electric injection and detection of spin transport in a non-local lateral spin valve, as demonstrated for the first time in the nonmagnetic metals at low-temperature by Jonson and Silsbee [10](single crystal Al bulk wire, below 77 K), and later at room-temperature by Jedema *et al*. [11, 12](mesoscopic Cu strips); in non-magnetic semiconductors at low-temperatures by Lou *et al*. [13](n-GaAs, below 70 K) and by van 't Erve *et al*. [14](n-Si, below 10 K), and later at room-temperature (RT) by Saito *et al*. [15](n-GaAs, RT), by Suzuki *et al*. [16](n-Si, RT), and by Tombros *et al*. [17](graphene, RT).

One can also measure the spin accumulation in a three-terminal geometry which is equivalent to the 4T non-local Hanle measurement geometry with L=0. See Appendix A for more details.

2.3.3 Two-terminal spin valve and Hanle measurements

In a two-terminal (2T) device, spin signals can be detected via the spin valve and the Hanle spin precession measurements, similar to the 4T nonlocal measurement geometry. However the difference is that in a 2T device, both contacts act as spin injectors and spin detectors (Fig. 2.3). The contacts are biased in such a way that one of them acts as spin injector and the other as spin extractor (see Section 2.2.4). When the bias is reversed, both contacts exchange their roles. Since the charge and spin current paths are same, the detected signal includes both the charge and the spin contributions.

For a current I passing through the circuit (Fig. 2.3), the voltage measured is given by,

$$V_{2t}(B) = V^{\rm C1}(B) - V^{\rm C2}(B) + IR^{\rm N}(B) \tag{2.23}$$

where $V^{\rm C1}$ and $V^{\rm C2}$ are the voltages that could be detected across the contacts C1 and C2, and $R^{\rm N}$ is the resistance of the N channel between the contacts. $P_{\rm in}^{\rm C1}$ denotes the injection polarization of contact $C1$.

The above equation V_{2t} can be written for parallel $\uparrow\uparrow$ and anti-parallel $\uparrow\downarrow$ configuration of the magnetization of contacts C1 and C2.

For the two terminal Hanle measurements, the total measured spin signal $\triangle R_{2t}(B) = \frac{V_{2t}^{\uparrow\downarrow}(B) - V_{2t}^{\uparrow\uparrow}(B)}{I}$ is given by,

$$\triangle R_{2t}(B) = \left[P_{\rm in}^{\rm C1}P_{\rm d}^{\rm C2} + P_{\rm d}^{\rm C1}P_{\rm in}^{\rm C2}\right]R^{\rm N}\Re\left\{\frac{e^{-\frac{L}{\lambda^{\rm N}}\sqrt{1+j\omega\tau}}}{\sqrt{1+j\omega\tau}}\right\} \tag{2.24}$$

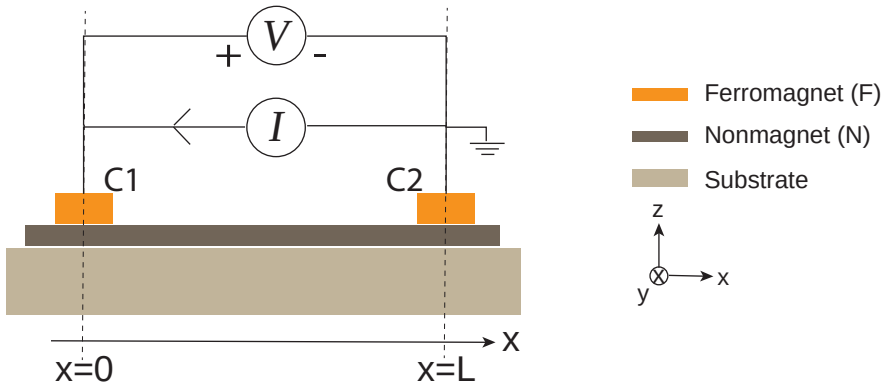

Figure 2.3: Two-terminal spin transport measurement geometry. Both the electrical spin injection and detection carried out using the same two contacts.

For two terminal spin valve measurements, $B_z = 0$, and the spin signal is measured while sweeping the magnetic field along the magnetization direction of the contacts. The resulting two-terminal spin valve signal $\triangle R_{2t}$ is given by,

$$\triangle R_{2t} = \left[P_{\text{in}}^{\text{C1}} P_{\text{d}}^{\text{C2}} + P_{\text{d}}^{\text{C1}} P_{\text{in}}^{\text{C2}}\right] R^{\text{N}} e^{-\frac{L}{\lambda^{\text{N}}}} \tag{2.25}$$

2.4 Spin conductivity mismatch

2.4.1 Transparent contacts

Let us consider the scenario where there is a small interface resistance of a contact (C), in other words, ohmic or transparent contact, i.e., $R^{\text{C}} \ll (R^{\text{F}}, R^{\text{N}})$, then, $P_{\text{in}}^{\text{C}} = \frac{P_{\sigma}^{\text{F}}}{1+\frac{R^{\text{N}}}{R^{\text{F}}}}$ (from Eq. 2.18). When the resistances of F and N are comparable, i.e., $R^{\text{N}} \approx R^{\text{F}}$, the spin polarization of the current penetrating into the N reduces moderately to half of the conductivity polarization of F, $P_{\text{in}}^{\text{C}} \approx \frac{P_{\sigma}^{\text{F}}}{2}$. However, when the resistance of N is higher than that of F, i.e., $R^{\text{N}} \gg R^{\text{F}}$, the injected current polarization reduces dramatically, $P_{\text{in}}^{\text{C}} \approx \frac{R^{\text{F}}}{R^{\text{N}}} P_{\sigma}^{\text{F}} \equiv \frac{\lambda^{\text{F}}}{\lambda^{\text{N}}} \frac{\sigma^{\text{N}}}{\sigma^{\text{F}}} \frac{P_{\sigma}^{\text{F}}}{1-P_{\sigma}^{\text{F}2}}$. Generally, for semiconducting N and metallic F, $\lambda^{\text{F}} \ll \lambda^{\text{N}}$ and $\sigma^{\text{N}} \ll \sigma^{\text{F}}$. As a result, P_{in}^{C} becomes small. This phenomenon has been observed experimentally in early attempts of spin injection into semiconductors through a direct contact of F [18–20]. The issue of a reduced efficiency of the spin polarization of the injected electrons from F to N is formulated as the *conductivity mismatch problem* [20]. The importance of the conductivity mismatch was first raised by Filip *et al*. [20] who explained that for an equal or higher conductivity of F compared to that of N, a very small spin polarization can be injected into N. This results in a

very small spin signal which can be difficult to detect. Moreover they suggested an alternate solution of using a semi-magnetic or ferromagnetic SC (also called Heusler compounds) as spin injection sources. However, these contacts are limited to low temperatures due to their Curie temperature and required high magnetic fields of the order of 1.5 T to polarize the contacts which would limit any practical applications, incorporating these materials.

2.4.2 Tunneling contacts

Later, a solution to the conductivity mismatch problem was proposed by Rashba [21], and Fert and Jaffres [22]. In order to overcome the conductivity mismatch condition, i.e., $\sigma^{N} \ll \sigma^{F}$ (or $R^{N} \gg R^{F}$), or to enhance the current spin injection polarization P_{in}^{C}, one needs even higher contact resistance of F/N interface, i.e., $R^{C} \gg (R^{F}, R^{N})$ [20–23]. This can be achieved by introducing a thin insulating (I) tunnel barrier at the F/N interface [24–26], i.e., by making a F/I/N tunnel junction one can limit the back flow of spins from N into F and restore the spin polarization to a significant level. In this case, the current spin injection polarization P_{in}^{C} (Eq. 2.18) is dominated by the spin dependent conductivity or the resistance of the barrier R^{C}, resulting in $P_{in}^{C} \approx P_{\sigma}^{C}$. In literature, P_{σ}^{C} is often refered to as spin asymmetry coefficient of the barrier γ [22], or tunneling spin polarization or simply, spin polarization in TMR experiments [27, 28]. Moreover, the conductivity mismatch problem can also be overcome by tuning a Schottky barrier at F/N interface [13, 29], or by forming a Zener-Esaki tunnel diode at F/N interface [30–33].

In case of spin injection into graphene, insertion of a tunnel barrier has been shown to increase the spin injection polarization [34]. The quality of the tunnel barrier and its interface morphology with graphene also play an important role in determining the spin injection efficiency [35] and the long distance spin transport [36]. More about this is discussed in Chapter 6.

2.5 Spin polarization

There are different methods developed for determining the spin polarization in various device systems: i)spin polarized tunneling or Meservey-Tedrow technique [37] for contact spin polarization in F/I/N tunnel junctions, ii)point contact Andrew reflection technique for measuring transport spin polarization of the F system [38–40], iii)spin wave Doppler technique [41] for measuring current polarization of a F, iv)spin-resolved photoelectron spectroscopy for DoS spin polarization (P_g) [42], v)time-resolved Faraday rotation experiments for measuring spin polarization of a semiconductor interfaced with a ferromagnet [43], and vi)spin valve and Hanle spin precession measurements in a lateral spin valve geometry [44] for measuring current

the spin polarization.

In the early works of spin polarized tunneling experiments [3, 37], it was explicitly assumed that the tunneling spin polarization is completely determined by the spin polarization of F electrodes. It was even predicted that the tunneling spin polarization is subjected to change by changing the tunnel barrier [45].

Various definitions of spin polarization of a material are given in the section 2.1. Generally, the current spin polarization of a material is defined as a ratio of the spin current I_s to the total charge current I flow, $P_j = \frac{I_s}{I}$. Often in literature [40], the current spin polarization of contact is defined as $\frac{\sigma^C_\uparrow - \sigma^C_\downarrow}{\sigma^C_\uparrow + \sigma^C_\downarrow}$, which is actually the conductivity spin polarization of the contact, P^C_σ (Eq. 2.14), and the current spin polarization of a F is defined as $\frac{g_\uparrow(E_F) - g_\downarrow(E_F)}{g_\uparrow(E_F) + g_\downarrow(E_F)}$, which is actually the density spin polarization of a F, P^F_g (Eq. 2.8). The definitions of P_σ and P_g are synonymously used for defining the current spin polarization P_j. From the definitions given by Eqs. 2.8, 2.7, 2.6, it is clear that P_g, P_σ, and P_j are inherently different. However, there is no direct way of measuring these spin polarizations.

In case of F, due to an exchange splitting between the up-spin and down-spin subbands, the spin DoS at the Fermi level are unequal, resulting in $P^F_\sigma \neq 0$. The current carried by the electrons in the bulk of F is spin polarized and the spin polarization of the current P^F_j is defined by Eq. 2.12.

In case of N, in equilibrium, the DoS at E_f of both spin subbands are equal and the current carried by the spins are equal. Thus the equilibrium current spin polarization and the equilibrium conductivity spin polarization in the bulk of N are zero, i.e., $P^N_\sigma = 0$, and $P^N_j = 0$. However, a small non-equilibrium spin accumulation can be created by injecting a spin polarized current in N which gives rise to a spin current flow and current spin polarization P^N_j, defined by Eq. 2.13.

For an F/N contact in a vertical F/N junction, shown in Fig. 2.1, the same formalism as above applies where P^C_σ and P^C_j are related by Eq. 2.15. Note that here, $P^C_\sigma \neq P^C_j$. Moreover, for an isolated vertical F/N contact the current spin injection polarization P^C_{in} and the spin extraction polarization are equivalent [46]. On the other hand, in a lateral non-local four-terminal geometry such as shown in Fig. 2.2, we can define two types of polarizations for a F/N contact; current spin injection polarization P^C_{in} and spin detection polarization P^C_d (Eq. 2.18). Note that, in contrast to the F/N contact in the vertical geometry[Fig. 2.1], the mechanism of spin injection and detection polarizations of a F/N contact in the nonlocal geometry[Fig. 2.2] are different due to separate paths for charge and spin currents. In other words, P^C_{in} can be written as a ratio of the spin current to the charge current across injector F/N contact, whereas, P^C_d can be defined as the ratio between the voltage detection to the spin accumulation underneath the detector F/N contact. Due to similar spin injection phenomenon in both vertical and nonlocal geometries, the current spin injection polarizations are same in these two geometries (Eqs. 2.15 and 2.18).

In the case of electrical spin injection experiments with high resistive tunnel barrier at a F/N interface i.e, $R^{C} \gg (R^{F}, R^{N})$, the *current spin injection polarization* becomes equal to the *conductivity spin polarization* of the contact, i.e., $P^{C}_{in} \sim P^{C}_{\sigma}$ (from Eq. 2.18). In literature, for the nonlocal spin transport experiments, these two polarizations are synonymously used, simply termed as *spin injection polarization*. Similarly, for the detector F/N contacts with a high resistive tunnel barrier, one can deduce $P^{C}_{d} \sim P^{C}_{\sigma}$, termed as *spin detection polarization*.

Moreover, due to a similar geometry of the F/N interface for the injector and the detector contacts in a nonlocal spin transport geometry, the detection polarization is assumed equal to the injection polarization [17], i.e., $P^{C}_{in} \equiv P^{C}_{d}$. However, the processes of electrical spin injection and detection are inherently different, and the both values P^{C}_{in} and P^{C}_{d} need to be considered separately for the nonlocal spin transport measurements

2.5.1 Bias dependence of spin polarization

As discussed in the previous section, insertion of a high resistive insulating (I) tunnel barrier at the F/N interface would overcome the conductivity mismatch problem. In such F/I/N contacts, the electrons will tunnel across the barrier whose spin conductivities ($\sigma^{C}_{\uparrow(\downarrow)}$) depend on the bias, say voltage (V), applied across the F/I/N tunnel junction. In a F/I/N tunnel junction with an high resistive tunnel barrier, $R^{C} \gg (R^{F}, R^{N})$, the majority of the voltage drop occurs across the barrier-channel interface. Therefore, the bias dependence of the spin conductivities $\sigma^{C}_{\uparrow(\downarrow)}(V)$ comes from the spin dependent conductivities of the ferromagnet and tunnel barrier, and possibly due to a magnetically proximity coupled N underneath the ferromagnetic contact [47–49].

One can experimentally observe the bias dependence of the spin injection and detection polarizations P^{C}_{in} and P^{C}_{d} in a nonlocal measurement geometry(see Chapter 6). The bias induced spin polarization has been reported in different tunneling F/I/N junctions, including (CoFe or NiFe)/Al_2O_3/Al/SiO_2 [50], Co/(1-3 layer)CVD-hBN/graphene/SiO_2 [51], Co/bilayer-hBN/graphene/hBN [52], and Co/two-layer-CVD-hBN/graphene/hBN [53].

2.5.2 Equivalent circuit for spin injection and detection

An equivalent circuit of the nonlocal measurement geometry of Fig. 2.2 is given in Figs. 2.4(a,b). Resistors in the unbiased($I = 0$) circuit represented by the symbol —▭— and the resistors in the biased($I \neq 0$) contacts are by —⧄—. In case of an unbiased measurements [Fig. 2.4(a)], the spin is injected with an AC current i and a voltage v is detected with the lock-in technique. In case of biased measurement, a DC current I_{in} is applied across the injector contacts along with a fixed magnitude of i

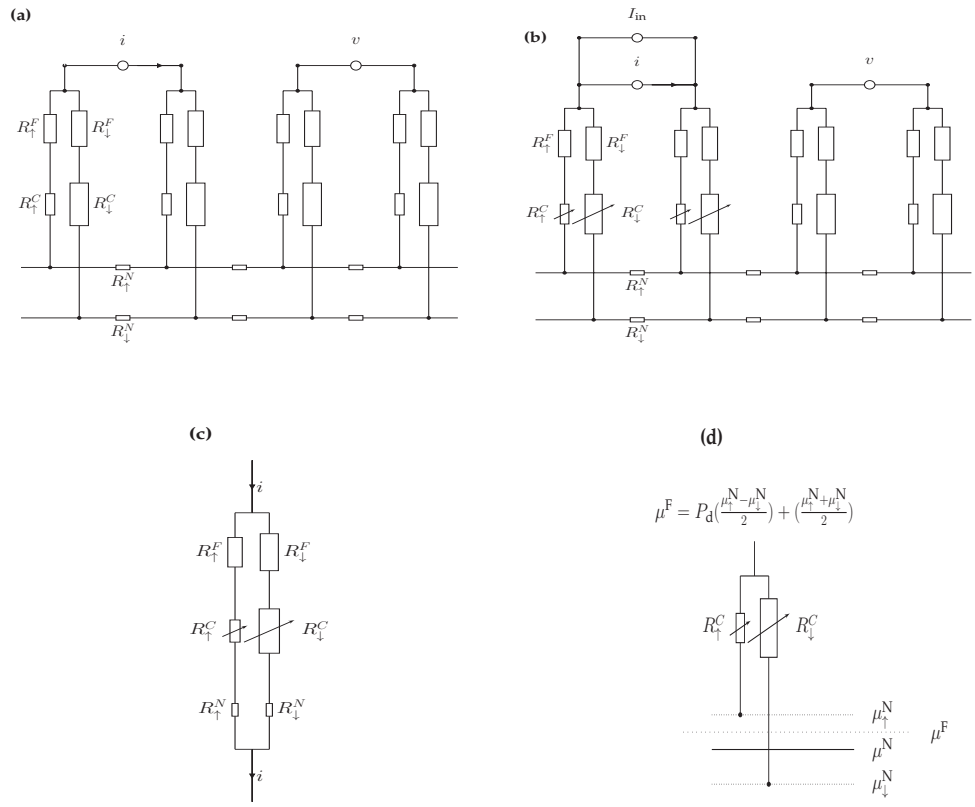

Figure 2.4: Equivalent resistor circuit of the nonlocal spin valve measurement geometry with (a) unbiased spin injection and detection contacts, (b) biased spin injection and unbiased spin detection contacts. Resistor model for (c) an injection contact and (d) detection contact. Each resistive element of the device is divided into up-spin and down-spin channels. For unbiased state, spin resistances of the contacts are constant. Whereas when a bias, for example, DC injection current I_{in} is applied, the spin resistances of the contacts change and thus result in change of the corresponding spin polarization. Here, the equivalent up(down)-spin resistances of F, C, and N of a F/N junction, near the interface region of length $\lambda^F + \lambda^N$, are given by $R^F_{\uparrow(\downarrow)} = \frac{\lambda^F}{\sigma^F_{\uparrow(\downarrow)}}$, $R^C_{\uparrow(\downarrow)} = \frac{1}{\sigma^C_{\uparrow(\downarrow)}}$, and $R^N_{\uparrow(\downarrow)} = \frac{2\lambda^N}{\sigma^N}$, respectively. The size of resistor box indicates the relative magnitude of up and down spin resistors.

and the measured v represents the differential change in the spin accumulation in N underneath the detector contact corresponding to the particular value of the injection bias I_{in}. One can also use a DC voltmeter across the detector contacts to measure the spin accumulation in N underneath the detectors corresponding to the spin injection by I_{in}, for a known detection polarization.

For the unbiased state[Fig. 2.4(a)], the spin resistances of a contact are nearly

constant. Whereas, for the biased state[Fig. 2.4(b)], the spin dependent resistances of a contact change whose spin dependent conductivities $\sigma^{\mathrm{C}}_{\uparrow(\downarrow)}(V)$ (or resistances $R^{\mathrm{C}}_{\uparrow(\downarrow)}(V)$) can be calculated from the Landauer-Büttiker formalism [54, 55]. Note that in case of a high resistive tunnel barrier contact, biasing across the F/N contact will also induce a gating effect for N underneath the contact [48].

Figure 2.4(c) shows the resistor circuit model of an injection contact. A general equation for the spin injection polarization P_{in} can be calculated from this circuit which is same as that of Eq. 2.15. The *differential spin injection polarization* $p_{\mathrm{in}}(I_{\mathrm{in}})$ of a contact at a particular injection bias I_{in} can be calculated by considering the differential resistances or conductivities of F, C, and N in Eq. 2.15[Fig. 2.4(a)].

Figure 2.4(d) represents the detection of spin accumulation in N using an F/N interface. In this detector contact, μ^{F} adjusts itself so that the total current in the detector is zero(Eq. 2.6), and is given by $\mu^{\mathrm{F}} = \mu^{\mathrm{N}} + P_{\mathrm{d}}\mu^{\mathrm{N}}_{\mathrm{s}}$, i.e., the chemical potential in F, μ^{F}, changes with respect to that of in N, μ^{N}, by a quantity proportional to the spin accumulation in N, $\mu^{\mathrm{N}}_{\mathrm{s}}$. The proportionality constant is the spin detection polarization $\mathrm{P_d}$. The detectable voltage $\mathrm{V_d}$ at this contact is the difference between the chemical potentials of F and N, i.e., $\mathrm{V_d} = \mu^{\mathrm{F}} - \mu^{\mathrm{N}}$. Therefore, the spin detection polarization of a contact can be defined as the ratio of the voltage that is being detected to the spin accumulation in N underneath the detector, $\mathrm{P_d}=\frac{V_{\mathrm{d}}}{\mu^{\mathrm{N}}_{\mathrm{s}}}$. If the measured voltage v probes the differential change in $\mu^{\mathrm{N}}_{\mathrm{s}}$, that is being created by the AC current i at a particular injection bias I_{in}, then the polarization is termed as *differential spin detection polarization* $p_{\mathrm{d}}(I_{\mathrm{in}})$.

2.6 Spin relaxation

Spin relaxation is a process in which the non-equilibrium spin accumulation depolarizes to reach at the equilibrium state. Therefore, materials in which the spin transport is less affected by the spin relaxation processes are attractive for spintronics applications. One of the key physical quantities for characterizing the spin transport in the solid state materials is the spin relaxation time which describes the non-equilibrium spin decay. How long a spin memory or spin information in a material can survive is determined by a time constant T1 and thus various spintronic device operations are limited to perform within this time scale.

In the original Bloch equations [56–58] used for describing the nuclear magnetic resonance, T1 is called thermal or longitudinal relaxation time, and T2 is called transversal relaxation time. The same equations can be used to describe the dynamics of the spin accumulation μ_{s} with τ_{s} being used in place of T_1 (in Eq. A.18b) and T_2 [in Eq. A.18a of Appendix A]. Here, T_1 is called longitudinal spin relaxation time, and T_2 is called transverse spin relaxation time or spin dephasing or decoherence time. The spins aligned along the direction of the external magnetic field are split

in the Zeeman energy which is exchanged with the lattice environment until the spins reach the equilibrium energy state. T_1 describes the decay of such spins to the equilibrium state. In the absence of an external magnetic field, T_1 describes the decay of non-equilibrium spin accumulation. Whereas, T_2 describes the decay of coherent oscillations of spins, which initially precess in-phase, perpendicular to the magnetic field.

The spin relaxation time can be determined by optical [59, 60] and all-electric [17, 61] measurements. The longitudinal spin relaxation time T_1 can be extracted in all-electric experiments by measuring the nonlocal spin valve signal $\triangle R_{\mathrm{s}}$ as a function of the distance L between the spin injector and detector contacts, using Eq. 2.22 with $\lambda^{\mathrm{N}} = \sqrt{DT_1}$ provided, spin polarizations of the involved contacts are same. T_2 can be obtained by fitting the experimentally measured nonlocal Hanle signal $\triangle R_{\mathrm{s}}(B)$ using Eq. 2.19 with $\lambda^{\mathrm{N}} = \sqrt{DT_2}$.

In graphene, the values of T_1 and T_2 are equal [17] in the absence of any external influence. Therefore, we use τ_{s} to denote the general spin relaxation time in accordance with literature. The following are the important spin relaxation mechanisms identified in metals and semiconductors [46, 59].

Elliott-Yafet mechanism: When the charge carriers scatter with impurities or phonons, the momentum scattering causes the spin flip. The spin flip events during the scattering result in a spin relaxation [62, 63]. The smaller the average time between the scatterings, faster the momentum scattering and more the chances of a spin flip, which leads to a smaller spin relaxation time, i.e., $\tau_{\mathrm{s}} \propto \tau_{\mathrm{p}}$ where τ_{p} is the momentum relaxation time.

D'yakonov-Perel' mechanism: Spin orbit coupling in a material results in a momentum dependent effective magnetic field which causes spin relaxation [64]. When the charge carriers scatter with impurities or phonons, they change their momentum or velocity. As a result they feel different spin orbit coupled magnetic field which is similar to the effect of an external magnetic field on a spin polarized current. Therefore the spin relaxation occurs in between the scattering events. The smaller the average time between the scatterings, smaller the spin precession, which means, larger the spin relaxation time, i.e., $\tau_{\mathrm{s}} \propto \tau_{\mathrm{p}}^{-1}$. Since the strength of the SOC is proportional to the fourth power of atomic number, Z^4, it is not a dominant spin relaxation mechanism for pure carbon based materials.

Hyperfine interactions: When the electrons are confined to a region with large number of nuclear spins, the hyperfine interactions of the nuclear spins with electrons lead to electron spin flip and electron spin dephasing. Morever, when the electrons are itinerant in the region of a nuclear spin, their random spin orientation gets nullified on an average [65]. Naturally available graphene is made of two stable isotopes, ^{12}C up to 99% and remaining 1% with ^{13}C. Only ^{13}C has nuclear magnetic moment. Therefore, the spin relaxation due to hyperfine interactions in graphene is also negligible.

References

[1] Valet, T. & Fert, A. Theory of the perpendicular magnetoresistance in magnetic multilayers. *Phys. Rev. B* **48**, 7099–7113 (1993).

[2] Fabian, J. *et al.* Semiconductor spintronics. *Acta Physica Slovaca* **57**, 565 907 (2007).

[3] Meservey, R. & Tedrow, P. M. Spin-polarized electron tunneling. *Physics Reports* **238**, 173–243 (1994).

[4] Johnson, M. & Silsbee, R. H. Coupling of electronic charge and spin at a ferromagnetic-paramagnetic metal interface. *Phys. Rev. B* **37**, 5312–5325 (1988).

[5] Sosenko, E., Wei, H. & Aji, V. Effect of contacts on spin lifetime measurements in graphene. *Phys. Rev. B* **89**, 245436 (2014).

[6] Jedema, F. J. *et al.* Electrical detection of spin accumulation and spin precession at room temperature in metallic spin valves. *Appl. Phys. Lett.* **81**, 5162–5164 (2002).

[7] Jedema, F. Electrical spin injection in metallic mesoscopic spin valves (2002). Relation: http://www.rug.nl/ date˙submitted:2003 Rights: University of Groningen.

[8] Takahashi, S. & Maekawa, S. Spin injection and detection in magnetic nanostructures. *Phys. Rev. B* **67**, 052409 (2003).

[9] Popinciuc, M. *et al.* Electronic spin transport in graphene field-effect transistors. *Phys. Rev. B* **80**, 214427 (2009).

[10] Johnson, M. & Silsbee, R. H. Interfacial charge-spin coupling: Injection and detection of spin magnetization in metals. *Phys. Rev. Lett.* **55**, 1790–1793 (1985).

[11] Jedema, F. J., Filip, A. T. & van Wees, B. J. Electrical spin injection and accumulation at room temperature in an all-metal mesoscopic spin valve. *Nature* **410**, 345–348 (2001).

[12] Jedema, F. J. *et al.* Electrical detection of spin precession in a metallic mesoscopic spin valve. *Nature* **416**, 713–716 (2002).

[13] Lou, X. *et al.* Electrical detection of spin transport in lateral ferromagnetsemiconductor devices. *Nature Phys.* **3**, 197–202 (2007).

[14] van t Erve, O. M. J. *et al.* Electrical injection and detection of spin-polarized carriers in silicon in a lateral transport geometry. *Appl. Phys. Lett.* **91**, 212109 (2007).

[15] Saito, T. *et al.* Spin injection, transport, and detection at room temperature in a lateral spin transport device with $Co_2FeAl_{0.5}Si_{0.5}$/n-GaAs schottky tunnel junctions. *Appl. Phys. Express* **6**, 103006 (2013).

[16] Suzuki, T. *et al.* Room-temperature electron spin transport in a highly doped Si channel. *Appl. Phys. Express* **4**, 023003 (2011).

[17] Tombros, N. *et al.* Electronic spin transport and spin precession in single graphene layers at room temperature. *Nature* **448**, 571–574 (2007).

[18] Lee, W. Y. *et al.* Magnetization reversal and magnetoresistance in a lateral spin-injection device. *J. Appl. Phys.* **85**, 6682–6685 (1999).

[19] Hammar, P. R. *et al.* Observation of spin injection at a ferromagnet-semiconductor interface. *Phys. Rev. Lett.* **83**, 203–206 (1999).

[20] Filip, A. T. *et al.* Experimental search for the electrical spin injection in a semiconductor. *Phys. Rev. B* **62**, 9996–9999 (2000).

[21] Rashba, E. I. Theory of electrical spin injection: Tunnel contacts as a solution of the conductivity mismatch problem. *Phys. Rev. B* **62**, R16267–R16270 (2000).

[22] Fert, A. & Jaffrès, H. Conditions for efficient spin injection from a ferromagnetic metal into a semiconductor. *Phys. Rev. B* **64**, 184420 (2001).

[23] Schmidt, G. *et al.* Fundamental obstacle for electrical spin injection from a ferromagnetic metal into a diffusive semiconductor. *Phys. Rev. B* **62**, R4790–R4793 (2000).

[24] Motsnyi, V. F. *et al.* Electrical spin injection in a ferromagnet/tunnel barrier/semiconductor heterostructure. *Appl. Phys. Lett.* **81**, 265–267 (2002).

[25] Jiang, X. *et al.* Highly spin-polarized room-temperature tunnel injector for semiconductor spintronics

using MgO(100). *Phys. Rev. Lett.* **94**, 056601 (2005).

[26] Dash, S. P. *et al.* Electrical creation of spin polarization in silicon at room temperature. *Nature* **462**, 491–494 (2009).

[27] Julliere, M. Tunneling between ferromagnetic films. *Physics Letters A* **54**, 225–226 (1975).

[28] Moodera, J. S. *et al.* Large magnetoresistance at room temperature in ferromagnetic thin film tunnel junctions. *Phys. Rev. Lett.* **74**, 3273–3276 (1995).

[29] Hanbicki, A. T. *et al.* Efficient electrical spin injection from a magnetic metal/tunnel barrier contact into a semiconductor. *Appl. Phys. Lett.* **80**, 1240 (2002).

[30] Makoto, K. *et al.* A spin Esaki diode. *Jpn. J. Appl. Phys.* **40**, L1274 (2001).

[31] Johnston-Halperin, E. *et al.* Spin-polarized Zener tunneling in (Ga,Mn)As. *Phys. Rev. B* **65**, 041306 (2002).

[32] Van Dorpe, P. *et al.* Very high spin polarization in GaAs by injection from a (Ga,Mn)As Zener diode. *Appl. Phys. Lett.* **84**, 3495 (2004).

[33] Ciorga, M. *et al.* Electrical spin injection and detection in lateral all-semiconductor devices. *Phys. Rev. B* **79**, 165321 (2009).

[34] Han, W. *et al.* Tunneling spin injection into single layer graphene. *Phys. Rev. Lett.* **105**, 167202 (2010).

[35] Józsa, C. *et al.* Controlling the efficiency of spin injection into graphene by carrier drift. *Phys. Rev. B* **79**, 081402 (2009).

[36] Gurram, M. *et al.* Spin transport in fully hexagonal boron nitride encapsulated graphene. *Phys. Rev. B* **93**, 115441 (2016).

[37] Tedrow, P. M. & Meservey, R. Spin-dependent tunneling into ferromagnetic nickel. *Phys. Rev. Lett.* **26**, 192–195 (1971).

[38] Nadgorny, B. *et al.* Transport spin polarization of Ni_xFe_{1-x}: Electronic kinematics and band structure. *Phys. Rev. B* **61**, R3788–R3791 (2000).

[39] Bouvron, S. *et al.* Andreev experiments on superconductor/ferromagnet point contacts. *Low Temperature Physics* **39**, 274–278 (2013).

[40] Chalsani, P. *et al.* Andreev reflection measurements of spin polarization. *Phys. Rev. B* **75**, 094417 (2007).

[41] Zhu, M., Dennis, C. L. & McMichael, R. D. Temperature dependence of magnetization drift velocity and current polarization in $Ni_{80}Fe_{20}$ by spin-wave Doppler measurements. *Phys. Rev. B* **81**, 140407 (2010).

[42] Dedkov, Y. S., Rüdiger, U. & Güntherodt, G. Evidence for the half-metallic ferromagnetic state of Fe_3O_4 by spin-resolved photoelectron spectroscopy. *Phys. Rev. B* **65**, 064417 (2002).

[43] Ciuti, C., McGuire, J. P. & Sham, L. J. Spin polarization of semiconductor carriers by reflection off a ferromagnet. *Phys. Rev. Lett.* **89**, 156601 (2002).

[44] Villamor, E. *et al.* Temperature dependence of spin polarization in ferromagnetic metals using lateral spin valves. *Phys. Rev. B* **88**, 184411 (2013).

[45] Beth Stearns, M. Simple explanation of tunneling spin-polarization of Fe, Co, Ni and its alloys. *J. Magn. Magn. Mater.* **5**, 167–171 (1977).

[46] Žutić, I., Fabian, J. & Das Sarma, S. Spintronics: Fundamentals and applications. *Reviews of Modern Physics* **76**, 323–410 (2004).

[47] Zollner, K. *et al.* Theory of proximity-induced exchange coupling in graphene on hBN/(Co, Ni). *Phys. Rev. B* **94**, 155441 (2016).

[48] Lazić, P., Belashchenko, K. D. & Žutić, I. Effective gating and tunable magnetic proximity effects in two-dimensional heterostructures. *Phys. Rev. B* **93**, 241401 (2016).

[49] Wu, Q. *et al.* Efficient spin injection into graphene through a tunnel barrier: Overcoming the spin-conductance mismatch. *Phys. Rev. Appl.* **2**, 044008 (2014).

[50] Valenzuela, S. O. *et al.* Spin polarized tunneling at finite bias. *Phys. Rev. Lett.* **94**, 196601 (2005).

[51] Kamalakar, M. V. *et al.* Inversion of spin signal and spin filtering in ferromagnet—hexagonal boron nitride-graphene van der Waals heterostructures. *Sci. Rep.* **6**, 21168 (2016).

[52] Gurram, M., Omar, S. & van Wees, B. J. Bias induced up to 100% spin-injection and detection polarizations in ferromagnet/bilayer-hBN/graphene/hBN heterostructures. *Nat. Commun.* **8**, 248 (2017).

[53] Gurram, M. *et al.* Spin transport in two-layer-CVD-hBN/graphene/hBN heterostructures. *Phys. Rev. B* **97**, 045411 (2018).

[54] Song, Y. & Dery, H. Spin transport theory in ferromagnet/semiconductor systems with noncollinear magnetization configurations. *Phys. Rev. B* **81**, 045321 (2010).

[55] Datta, S. *Electronic Transport in Mesoscopic Systems* (Cambridge University Press, 1997).

[56] Bloch, F. Nuclear induction. *Phys. Rev.* **70**, 460–474 (1946).

[57] Carr, H. Y. & Purcell, E. M. Effects of diffusion on free precession in nuclear magnetic resonance experiments. *Phys. Rev.* **94**, 630–638 (1954).

[58] Torrey, H. C. Bloch equations with diffusion terms. *Phys. Rev.* **104**, 563–565 (1956).

[59] Meier, E. F. & Zakharchenya, B. Optical orientation: Modern problems in condensed matter sciences. *Science* **8**, 1–523 (1984).

[60] Kuzma, N. *et al.* Ultraslow electron spin dynamics in GaAs quantum wells probed by optically pumped NMR. *Science* **281**, 686–690 (1998).

[61] Žutić, I., Fabian, J. & Sarma, S. D. Proposal for all-electrical measurement of T1 in semiconductors. *Appl. Phys. Lett.* **82**, 221–223 (2003).

[62] Elliott, R. J. Theory of the effect of spin-orbit coupling on magnetic resonance in some semiconductors. *Phys. Rev.* **96**, 266–279 (1954).

[63] Yafet, Y. g factors and spin-lattice relaxation of conduction electrons. *Solid state physics* **14**, 1–98 (1963).

[64] Dyakonov, M. & Perel, V. Spin relaxation of conduction electrons in noncentrosymmetric semiconductors. *Soviet Physics Solid State, Ussr* **13**, 3023–3026 (1972).

[65] D'Yakonov, M. I. & Perel', V. I. Optical orientation in a system of electrons and lattice nuclei in semiconductors. Theory. *Sov. Jour. Exp. and Theor. Phys.* **38**, 177 (1974).